Journal of Physics: Photonics

OPEN ACCESS

RECEIVED
23 March 2026

REVISED
13 May 2026

ACCEPTED FOR PUBLICATION
10 June 2026

PUBLISHED
3 July 2026

PAPER

Chirped pulse analysis and control in non-Hermitian scattering systems using complex time delay

Isabella L Giovannelli[1,*], **Steven M Anlage**[1,2] **and Thomas M Antonsen**[2]

[1] Quantum Materials Center, Department of Physics University of Maryland, College Park, MD 20742, United States of America
[2] Department of Electrical and Computer Engineering University of Maryland, College Park, MD 20742, United States of America
[*] Author to whom any correspondence should be addressed.

E-mail: igiovann@umd.edu

Keywords: complex time delay, pulse shaping, chirped pulses, pulse propagation, linear scattering systems, dispersive systems

Supplementary material for this article is available online

Abstract

We theoretically and experimentally establish a connection between linearly chirped pulse propagation properties and the complex generalization of Wigner–Smith time delay for both transmitted and reflected pulses in linear and dispersive reverberant non-Hermitian scattering systems. We demonstrate that the time shift of the chirped pulse depends on both the real and imaginary parts of the complex time delay (CTD) of the scattering system. We also show that the chirped pulse experiences a center frequency shift that is directly proportional to the imaginary component of CTD, similar to that found in Giovannelli *et al* (2025 *Phys. Rev. Lett.* **135** 043801). Using these insights, we then demonstrate how CTD can be harnessed to systematically tune the propagation properties of a chirped pulse such that a near-zero time shift can be achieved for a wide range of pulse center frequencies in a resonant scattering system. Overall, this work broadens the utility and establishes the physical significance of complex time delays in non-Hermitian settings.

1. Introduction

Chirped pulses are pulses whose instantaneous frequency varies throughout the pulse. They are the basis for multiple modern technologies and are present in various physical phenomena. A nonexhaustive list includes chirped pulse amplification [1]; chirped pulse interferometry [2, 3] and spectroscopy [4, 5]; lidar, radar, and sonar [6–13]; fiber optics and photonics [7, 12–19]; frequency domain reflectometry [8, 20]; attosecond pulse control [21–23]; qubit control [20, 24–26]; wireless communication [27, 28] and biological/medical imaging [29–33]. Chirped pulses are widely utilized for their ability to be compressed and expanded without altering their frequency bandwidth. This allows for ultrashort intense pulses to be safely amplified without changing their spectrum. This also allows for the creation of long pulses with large frequency bandwidths which then provide long range high resolution measurements that are robust against dispersion. These advantages are what have made chirped pulses so versatile. In all these applications, it is imperative to have precise control over the propagation of a chirped pulse through a given scattering environment, particularly its time delay.

In this paper we focus on understanding and controlling the time delay of linearly chirped pulses. In particular we are concerned with *linear* pulse propagation through a non-Hermitian lossy dispersive system where the incident waves can be related to the output waves via the transmission or reflection matrix [34, 35]; defined as sub-matrices of the scattering matrix (S). This work strives to create a connection between the behavior of chirped pulses in non-Hermitian scattering systems and a version of Wigner–Smith time delay [36–38] adapted for non-Hermitian settings [35, 39]. In this context, we use the term non-Hermitian to indicate that we are working with open dissipative systems, as established in the photonics and wave-scattering literature [40–43].

In this paper we use an extension of Wigner–Smith time delay [36–38] to describe how long a wave lingers in a non-Hermitian scattering system. Wigner–Smith time delay was originally defined

in the context of unitary nuclear scattering and was later generalized to include non-unitary dispersive scattering systems in the context of classical electromagnetic waves [35, 39]. We use this extension, referred to as complex time delay (CTD) or non-Hermitian Wigner Smith Time delay, to predict the time shift of a chirped electromagnetic pulse after it travels through a resonant scattering system. CTD is expressed as,

$$\tau = \frac{-\mathrm{i}}{2\pi}\frac{\partial}{\partial f}\ln[\rho(f)] = \mathrm{Re}[\tau] + \mathrm{iIm}[\tau] \tag{1}$$

where τ is complex time delay, ρ represents either $det[S]/M$ (Wigner–Smith), or a scattering matrix transmission (T) or reflection (R) coefficient of S, f is frequency, and M is the number of scattering channels. This generalization of time delay is complex due to the sub-unitary and dispersive nature of $det[S]$ and the matrix elements [35, 39, 44–47]. This can be seen by representing complex $\rho(f)$ in terms of a frequency dependent magnitude and phase. The real and imaginary parts of these delays can be positive, negative or zero. The use of CTD is general in the sense that it requires no symmetries of the Hamiltonian (e.g. Parity-Time [48]) or scattering matrix (e.g. reflection symmetry [49]). We have established that CTD is equally valid in the context of both reciprocal and non-reciprocal scattering systems [47, 50]. Wigner–Smith time delay is one specific case of the Generalized Wigner–Smith Operator (GWSO) which has been developed as a model for scattering control with a wide range of applications directed towards non-Hermitian systems [51–54].

There has been considerable effort to understand the physical meaning behind negative real time delay, or fast light, measured with Gaussian pulses [55–60]. This phenomenon occurs when the group velocity of light is either greater than the speed of light in vacuum, or negative. This happens, for example, in scattering systems near/at a resonance where there is a large amount of anomalous dispersion [58]. These cases have been observed experimentally [59, 61] and are both interpreted as the result of extreme nonuniform attenuation of the Fourier components of the pulse as it travels through the anomalously dispersive medium. Note that the general pulse shape is not distorted as long as the frequency bandwidth of the pulse is less than the width of the resonance being excited in the system [55, 58]. The nonuniform change in the Fourier components leads to a shift in time of the pulse peak, creating the illusion that the pulse has left the system before it has entered [56, 58]. This does not violate causality since there is a distinction between group velocity and information velocity as explained by Sommerfeld and Brillouin [62–64] and experimentally demonstrated in reference [61]. There has also been recent work on interpreting negative time delay in quantum mechanical systems, where in [65, 66] they explore the time delay of a photon traveling through an atom cloud.

Imaginary time delay has received considerably less attention than negative time delay/fast light. Imaginary transmission time delay was first properly predicted to correspond to a center frequency shift in a Gaussian pulse in [44], and experimentally confirmed in [69]. Imaginary time delay occurs for the same reason that negative time delay does: it is the result of nonuniform distortion of the Fourier components as the pulse travels through an anomalously dispersive linear medium.

In previous work [44, 69], the relationship established between CTD derived from frequency-domain scattering parameters, and the time-domain pulse propagation properties, were only established for Gaussian wave packets. We now wish to generalize these CTD results to chirped pulses, which are of great interest to many different fields and applications. Here we theoretically and experimentally demonstrate how the properties of a chirped pulse change as it travels through a linear non-Hermitian dispersive scattering system. We also show how these changes in pulse propagation properties can be accurately predicted with only knowledge of the complex transmission (or reflection) coefficient as a function of frequency. Further, we analyze how the peak of the chirped pulse shifts in time as well as how its center frequency changes after it travels through a non-Hermitian scattering system. We then demonstrate that these shifts are directly related to the corresponding CTD (reflection or transmission). Specifically, we confirm that the frequency shifts are directly proportional to imaginary time delay in a manner similar to that shown in [44, 69]. We also show that the peak time shifts of a chirped pulse depend not only on the real part of CTD but also in a non-trivial way on the imaginary part.

2. Chirped pulse properties and CTD

The predicted results connecting CTD and chirped pulse properties can be derived following a process similar to that utilized in [44, 67, 69]. The details of this calculation can be found in the supplementary

materials. We define a linearly chirped pulse to be the following:

$$E_i(t) \propto \exp\left[-\mathrm{i}2\pi f_0 t - \left(\mathrm{i}\Omega' + \delta_t^{-2}\right)\frac{t^2}{2}\right] \tag{2}$$

where f_0 is the center frequency of the pulse, Ω' is the linear chirp rate and $\delta_t = \frac{\delta_T}{2\sqrt{2\ln 2}}$ where δ_T is the full width at half maximum of the amplitude of the pulse in the time domain. The frequency bandwidth of the chirped pulse is subsequently defined as,

$$\delta_f = \frac{1}{\pi}\sqrt{2\ln 2\left(\Omega'^2\delta_t^2 + \delta_t^{-2}\right)} \tag{3}$$

where δ_f is the FWHM of the chirped pulse amplitude in the frequency domain in Hz. Note that in this formulation of a chirped Gaussian pulse, the chirp rate is bounded by the chosen frequency bandwidth of the pulse,

$$\Omega' \leqslant \frac{\left(\pi\delta_f\right)^2}{4\ln 2} \tag{4}$$

The explanation for this bound is contained in section 2 of the supplementary materials.

We consider the case of a pulse propagating through a linear dispersive system for which the pulse frequency bandwidth (equation (3)) is much smaller than the 3 dB linewidth of the chosen resonance of the scattering system. Note that we treat the scattering system in terms of its dispersive overall transmission/refection coefficient, rather than as a continuous extended medium in space. We define the shifts in frequency and time to be the shifts in frequency of the peak of the power spectral density, and shifts in time of the peak of the pulse power, respectively. These are directly related to the CTD of the scattering system. The shift in center frequency is predicted to be,

$$D_f = -\tilde{\Delta}^2\mathrm{Im}[\tau] \tag{5}$$

where D_f is the shift in center frequency in Hz and $\tilde{\Delta} = \frac{1}{2\pi}\sqrt{\Omega'^2\delta_t^2 + \delta_t^{-2}} = \frac{\delta_f}{2\sqrt{2\ln 2}}$ is proportional to the bandwidth of the chirped pulse. The time shift in the output pulse is found to be,

$$D_t = \mathrm{Re}[\tau] - \Omega'\delta_t^2\mathrm{Im}[\tau] \tag{6}$$

where D_t is the predicted time shift of the chirped pulse which, surprisingly, depends on the imaginary part of time delay, in addition to the real part, weighted by a factor of the chirp time-bandwidth product $\Omega'\delta_t^2$. This allows for an extraordinary degree of control of D_t, as demonstrated in figure 6, where we achieve the $D_t = 0$ condition over a broad range of pulse center frequencies.

3. Experiment

The time domain experiment setup is depicted in figure 1, where we use a signal generator to create a chirped pulse that is sent through the resonant system and then measured on an oscilloscope. In more detail, a chirped pulse is produced using a 50 GSa s^{-1} Tektronix model AWG70001B arbitrary waveform generator (AWG). The time domain expression used to define the chirped pulse is given by the imaginary part of equation (2). The two output ports on the AWG (1+, 1-) produce nominally identical pulses that are sent through twin 33.02 cm-long coaxial cables. Port 1- is connected directly to channel 2 of a Keysight/Infiniium model UXR0104A 25 GHz bandwidth real-time digital sampling oscilloscope, which captures the "measured input pulse". Port 1+ of the AWG is connected to the resonator. The output pulse from the resonator is then measured on channel 4 of the oscilloscope. Lastly, the orange cable connects the AWG marker channel (M1+) to channel 1 of the oscilloscope and acts as the trigger signal. We note that Port 1- is the differential complement of Port 1+. The pulses coming out of these ports need to be identical in order to have a valid comparison between the pulse that travels through the "measured input cable" and the pulse that travels through the whole system. We meet this condition by simply multiplying the output signal from Port 1- by -1.

In a separate experiment, the complex transmission $T(f)$ and reflection $R(f)$ coefficients of the ring resonator were measured using a Keysight N5242A network analyzer (PNA-X) that is calibrated using a Keysight N4691-60 001 Electronic Calibration kit at the resonator's connection points. The measured transmission coefficient magnitude shown in figure 2(a) is taken over the frequency range 0.1 GHz to 1

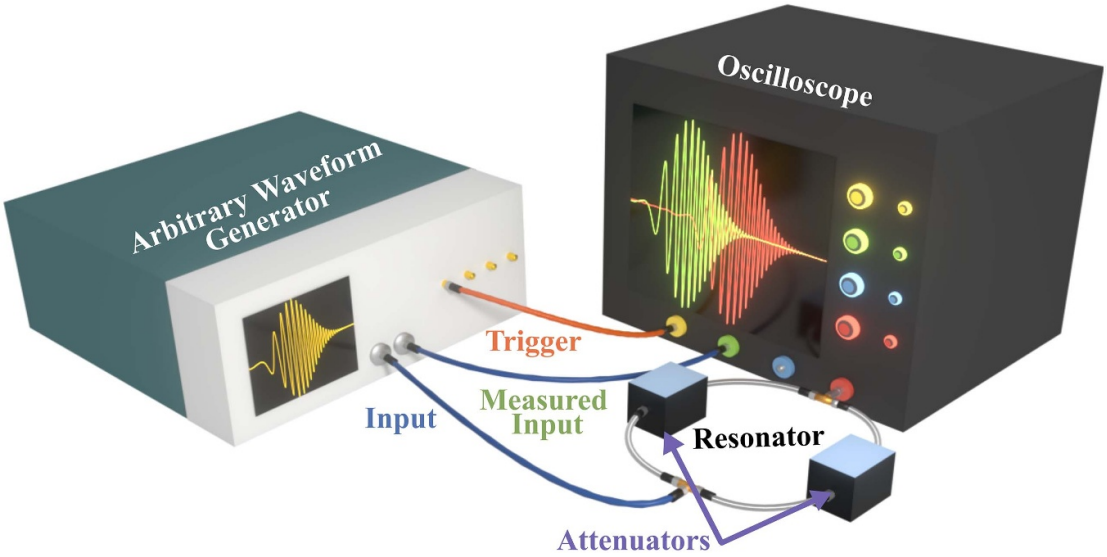

Figure 1. Schematic of time domain experiment setup. The ring resonator depicted is the one that was used for the transmission case.

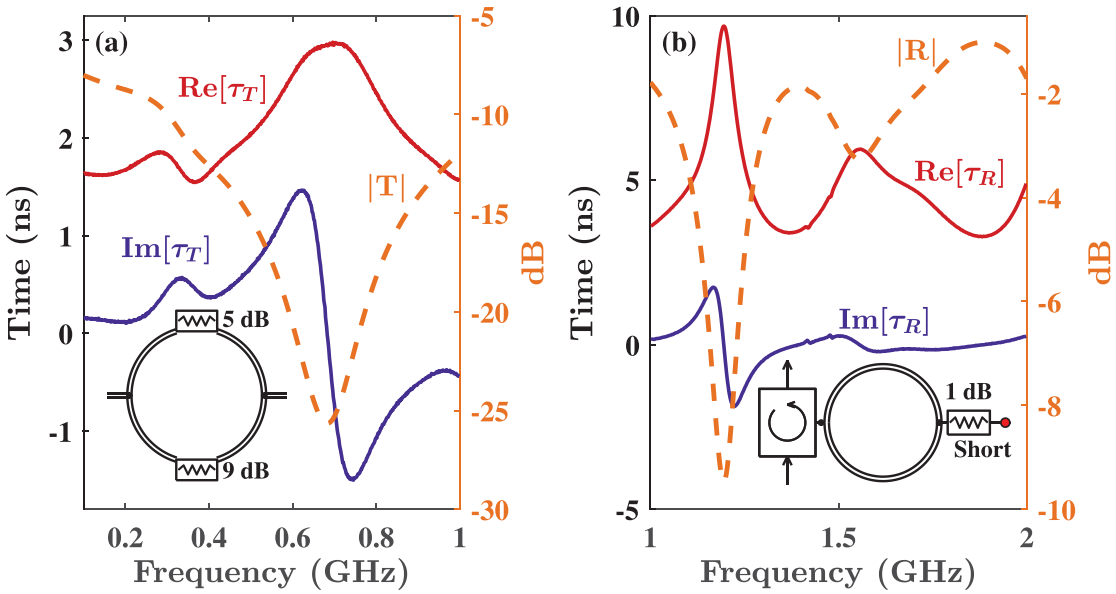

Figure 2. (a) The transmission scattering parameter (dashed orange, right axis), real (red) and imaginary (purple) parts of the transmission complex time delay (left axis). A schematic of the transmission resonator is depicted in the lower left. (b) The reflection scattering parameter (dashed orange) and real (red) and imaginary (purple) parts of reflection complex time delay. A schematic of the resonator used for the reflection case is depicted in the lower right, where the block containing a circular arrow is a circulator.

GHz with a frequency step size of 1.331 MHz. The reflection coefficient magnitude shown in figure 2(b) was measured over the frequency range of 1 GHz to 2 GHz with a frequency step size of 1.66 MHz. The corresponding real and imaginary parts of complex transmission and reflection time delay calculated using equation (1), are shown as solid lines in figure 2.

The transmission and reflection measurements were performed using the same experimental setup, but with two different resonators. Different resonators were used in the two cases to establish wide resonances of comparable size, which then provided similarly sized large D_t and D_f values for transmission and reflection, which are shown in figures 4 and 5, respectively. The transmission resonance is situated at 0.684 GHz and has a 3 dB frequency bandwidth of about 117 MHz. The reflection resonance is centered at 1.19 GHz with a 3 dB bandwidth of 82 MHz.

The resonator used in the transmission case was a dispersive microwave ring resonator [35, 68] consisting of 4 coaxial cables and 2 identical Narda (model 4745-69) step attenuators, as shown in the lower

left of figure 2(a). These attenuators create additional loss and dissipation in order to widen the resonant modes of the system. Two of the cables are each 15.24 cm-long and are attached to either side of a step attenuator set at 5 dB. The other two cables are each 7.62 cm-long and are attached to either side of the other step attenuator set at 9 dB. The ring is completed with two 'tee' junctions, creating a 2-port network. This resonator is reciprocal, allowing us to say $\tau_{12} = \tau_{21}$, hence we only refer to one transmission coefficient (T) when describing the system. The symmetry in this system does not play a pivotal role in the theory or results we present. The simple experimental design was chosen to allow for clear interpretation of the results. See [48, 49] for how symmetry can play a role in non-Hermitian scattering systems.

The ring resonator used for the reflection case is depicted on the lower right of figure 2(b). It is composed of a 1–2 GHz Pasternack model PE83CR003 microwave circulator that is connected through a 'tee' junction to two identical 12.7 cm-long coaxial cables forming a ring with a Narda (model 4745-69) attenuator set to 1 dB connected with a 'tee' junction on the other side. The opposing port on the attenuator was connected to a short circuit to encourage the wave to make a round trip through the attenuator before returning to the ring. One port of the circulator is the input, while the output was connected to a male-to-male adapter that was directly connected to the oscilloscope. All of the elements in this resonator are lossy and add dissipation to the system.

4. Data and discussion

Figure 3 shows normalized raw transmitted pulse data of a few representative measured input and output pulses, their corresponding Fourier transforms, and the time/frequency shifts extracted from the data. The input pulses are in dark blue and the corresponding outputs are in yellow. Panels (a) and (c) of figure 3 correspond to a pulse with center frequency $f_c = 0.1013$ GHz and a chirp rate of $\Omega' = 3.39\ \frac{\text{MHz Rad}}{\text{ns}}$. This pulse has a time width (δ_t) of 54.89 ns, a frequency bandwidth (δ_f) of 70 MHz, and a chirp factor ($\Omega'\delta_t^2$) of 10.20. This serves as an example of a pulse with both a minimum transmission time shift ($D_t = 0.10 \pm 0.03$ ns) and a minimum center frequency shift ($D_f = -0.8479 \pm 0.0140$ MHz). (The uncertainty estimates are detailed in the Supp. Mat.) Panels (b) and (c) of figure 3 correspond to a pulse from the data shown in figure 4(b) with a center frequency of 0.6157 GHz, which situates it right near peak resonance. The insets on either side of the pulse are zoomed-in regions of detailed oscillations to illustrate that the pulse is not just a Gaussian pulse but a chirped Gaussian pulse. The pulse has a chirp rate of 0.071 $\frac{\text{MHz Rad}}{\text{ns}}$, and a pulse length ($\delta_t$) of 3.75 μs. This is an example of a pulse that undergoes both a large negative time shift ($D_t = -1.2904 \pm 0.0001\,\mu$s) and a large negative frequency shift ($D_f = -14.6576 \pm 0.0006$ MHz). The transmission times (t_c) and center frequencies (f_c) are depicted as vertical lines in figure 3, and are calculated using the first temporal moment of the pulse, as done in reference [69]. This is valid when working in the small bandwidth limit where the frequency bandwidth of the pulse is less than the 3 dB bandwidth of the excited resonance, hence higher-order terms in the phase and attenuation vs frequency expressions can be neglected (see Supp. Mat. Section 1). The pulse in panels (a) and (c) has a frequency bandwidth of 70 MHz, and the pulse in panels (b) and (d) has a bandwidth of 100 MHz which are both smaller than the width of the transmission resonance (117 MHz).

The main results comparing the measured time and frequency shifts with the predictions made in equations (5)–6 are shown in figures 4 and 5, for transmission and reflection, respectively. The time-domain transmission data consists of 93 data points taken over the pulse center frequency range 0.1–1 GHz and the reflection time-domain data consists of 32 data points taken over 1–2 GHz. The symbols show the time-domain D_t and D_f measurements, while the solid lines show quantities constructed from frequency-domain data to test equations (5) and (6). Shown are data from a variety of pulses with different bandwidths δ_f and chirp rates $\Omega'\delta_t^2$ (positive and negative). From this we see that the predictions are consistent with the experimental results for a variety of pulse frequency bandwidths and chirp parameter values. We see that the frequency shifts (D_f) scale with the pulse frequency bandwidth squared, as expected from equation (5). We also see that there is less agreement for large frequency bandwidths as they approach the 3 dB-linewidth of the resonance being excited. This is expected as this is where the theory starts to break down (see Supp. Mat. Section 1). This was the main motivation for designing resonators to have wide modes so that we could achieve such large frequency shifts. As the pulse frequency bandwidth approaches the width of the resonance, the measured time and frequency shifts decrease, eventually approaching zero for an isolated mode. This case is demonstrated in figure 3(b), (d) of the supplementary materials of reference [69]. This behavior is also partially demonstrated in figure 4(c) and figure 5(c) where we see that at larger bandwidths the measured pulse shifts decrease in amplitude in comparison to the shifts predicted by frequency domain CTD.

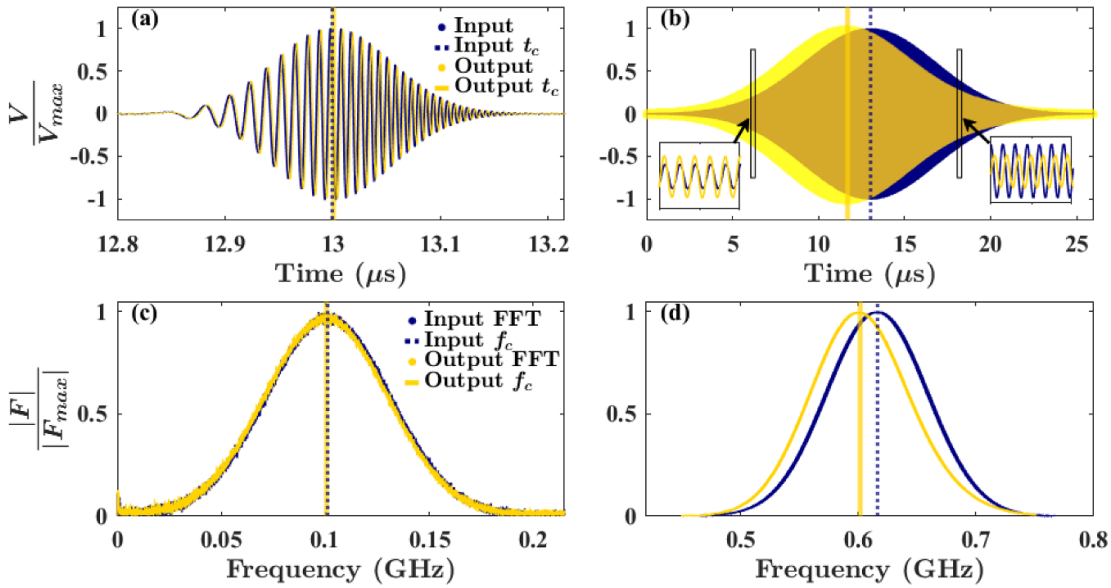

Figure 3. Panels (a) and (b) are examples of the time domain chirped pulses sent through the resonator depicted in figure 1. The pulses sent into the resonator are plotted in blue and the output pulses are plotted in yellow. The transmission times are calculated as the mean of the envelope of the pulse ($t_c = \int |V(t)|^2 t\,\mathrm{d}t / \int |V(t)|^2\,\mathrm{d}t$) and are shown as corresponding vertical lines. The solid yellow vertical line is the transmission time of the output pulse and the dashed blue vertical line is the transmission time of the input pulse. The Fourier transforms (FFTs) of the pulses in (a) and (b) are depicted in panels (c) and (d) respectively. The calculated center frequencies $\left(f_c = \int |F(f)|^2 f\,\mathrm{d}f / \int |F(f)|^2\,\mathrm{d}f\right)$ are marked on the plots as vertical lines: solid yellow for the output pulse center frequency and dashed blue for the input pulse center frequency. Panels (a) and (c) are an example of chirped pulse with an extremely small magnitude time and frequency shift (from data set depicted in figure 6(a)). Panels (b) and (d) are an example of a pulse with a large time and center frequency shift from the dataset depicted in figure 4(b). The insets in (b) show detailed oscillations of the pulses in equal-width (10 ns) time windows, illustrating the chirped nature of the pulse.

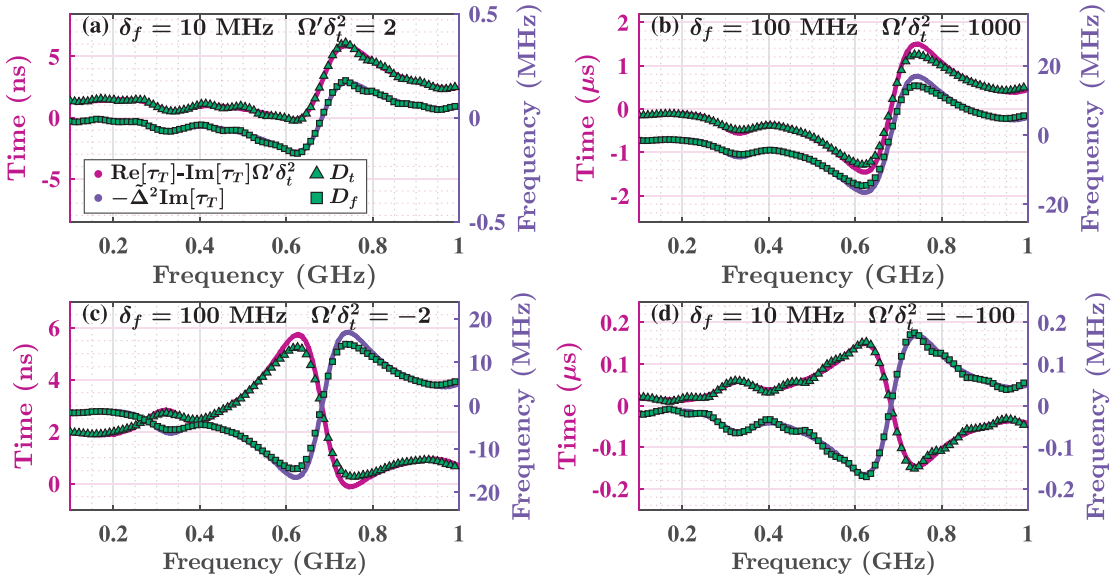

Figure 4. Summary of measured and expected transmission time delays and frequency shifts for chirped pulses having various $\Omega'\delta_t^2$ and δ_f values, as a function of center frequency. The predicted time shift is plotted in magenta and the measured pulse time shift are the green triangles. The predicted frequency shift is in light purple and the measured pulse frequency shift is plotted as green squares. The chirp rates and pulse widths used are as follows: (a) $\Omega' = 0.2848\ \frac{\mathrm{MHz\,Rad}}{\mathrm{ns}}$ and $\delta_t = 83.8$ ns, (b) $\Omega' = 0.0712\ \frac{\mathrm{MHz\,Rad}}{\mathrm{ns}}$ and $\delta_t = 3747.82$ ns, (c) $\Omega' = -28.48\ \frac{\mathrm{MHz\,Rad}}{\mathrm{ns}}$ and $\delta_t = 8.38$ ns, (d) $\Omega' = -0.0071\ \frac{\mathrm{MHz\,Rad}}{\mathrm{ns}}$ and $\delta_t = 3748$ ns.

Note that the case of an un-chirped pulse is included for reflected pulses in figure 5(b). This case was not reported in reference [69], and is demonstrated for the first time here. Additional data for the pulse reflection case is included in Supp. Mat. Section 3.

It is clear from the data that the time shift of the pulse is heavily dependent on the magnitude of the dimensionless chirp parameter $\Omega'\delta_t^2$. We see that in both transmission and reflection, the time shift

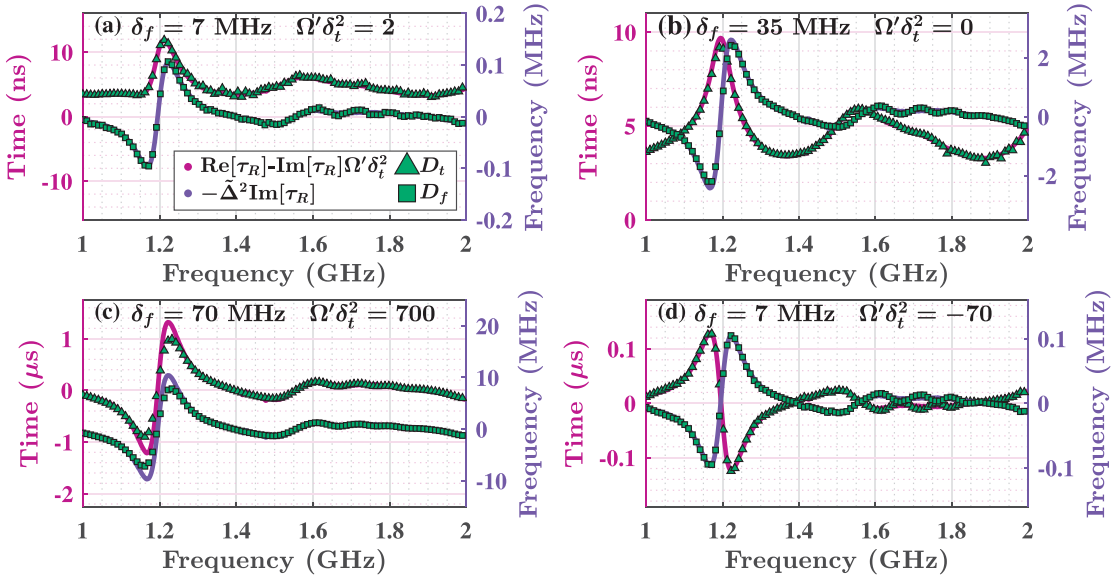

Figure 5. Summary of measured and expected time shifts and frequency shifts for chirped pulses after reflection from a ring resonator. The predicted center frequency shifts are shown in in light purple, and predicted time shifts in magenta with the measured frequency shifts represented as green rectangles and time shifts represented as green triangles. This is done for various chirped pulse frequency bandwidths (δ_f) and $\Omega'\delta_t^2$ values. The chirp rates and pulse widths used are as follows: (a) $\Omega' = 0.1395\ \frac{\mathrm{MHz\,Rad}}{\mathrm{ns}}$ and $\delta_t = 120$ ns, (b) $\Omega' = 0\ \frac{\mathrm{MHz\,Rad}}{\mathrm{ns}}$ and $\delta_t = 10.71$ ns, (c) $\Omega' = 0.0498\ \frac{\mathrm{MHz\,Rad}}{\mathrm{ns}}$ and $\delta_t = 3747.80$ ns, (d) $\Omega' = -0.005\ \frac{\mathrm{MHz\,Rad}}{\mathrm{ns}}$ and $\delta_t = 3747.87$ ns.

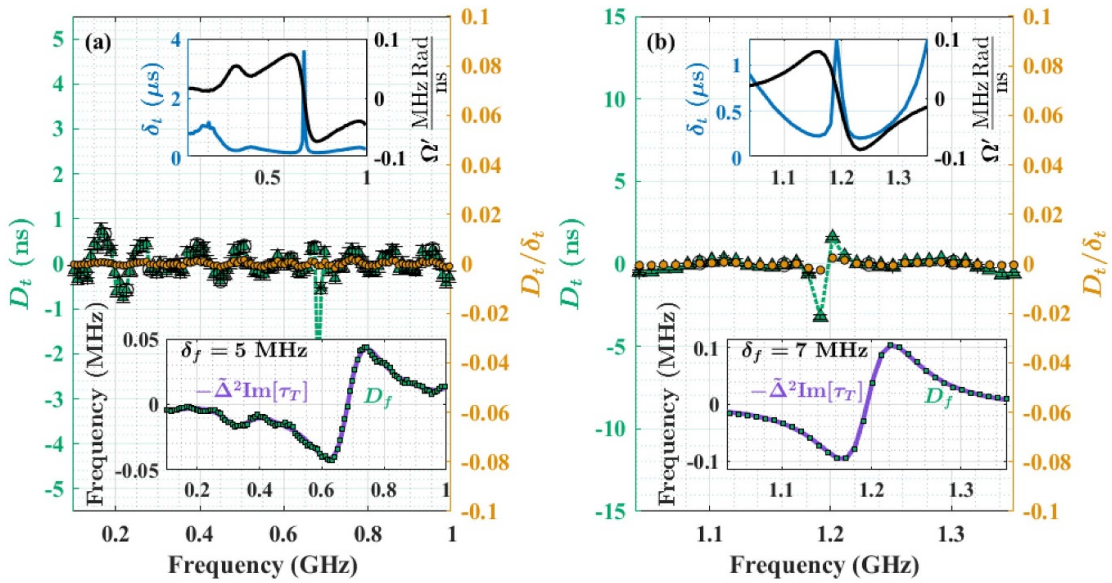

Figure 6. Results for the case where the chirped-pulse temporal shift D_t is zeroed out by setting $\mathrm{Re}[\tau]/\mathrm{Im}[\tau] = \Omega'\delta_t^2$ at each choice of center frequency. Panels (a) and (b) are the results for transmission and reflection, respectively. The green triangles correspond to the measured chirped pulse transmission (a) and reflection (b) time shift (left axis). The light orange circles correspond to time-shift normalized to the width of the pulse (right axis). The lower insets in (a) and (b) show the predicted and measured center frequency shifts plotted in light purple and as green squares, respectively, along with the value of the common pulse bandwidth δ_f. The upper insets show the chosen values of δ_t and Ω' versus center frequency utilized to achieve $D_t = 0$ for the chirped pulse.

jumps from being on the scale of nanoseconds to microseconds, scaling with $\Omega'\delta_t^2$. We note that in the limit of large $\Omega'\delta_t^2$, and/or large $\mathrm{Im}[\tau]$, D_t converges to a frequency dependence that is identical to that of D_f (modulo a sign). This makes sense when looking at equation (6) where the imaginary part of time delay is expected to dominate the time shift in the chirped pulse when $\Omega'\delta_t^2$ is large. This is also true for the negative chirp case, except for a minus sign, following the sign of the chirp rate (as demonstrated in figures 4(c)–(d) and 5(d)).

In figure 6 we demonstrate how with knowledge of CTD one can manipulate the chirped pulse properties such that the time shift of the pulse is zero over a broad range of center frequencies. Combining equations (6) and (3) allows one to choose unique values for δ_t and Ω', for a given pulse bandwidth δ_f, such that $\mathrm{Re}[\tau]/\mathrm{Im}[\tau] = \Omega'\delta_t^2$, resulting in a zero time shift $D_t = 0$ of the chirped pulse. (Note that one must choose new values of $\Omega'\delta_t^2$ at each pulse center frequency because $\mathrm{Re}[\tau]$ and $\mathrm{Im}[\tau]$ are frequency dependent.) We tested this experimentally for both transmission and reflection, and the results are shown in figure 6. Shown there are the time shifts D_t (green symbols) over a broad range of pulse center frequency, for both transmission and reflection. The average D_t value over the bandwidth found for the transmission case in figure 6(a) is -0.03 ± 0.12 ns, which is a shift in time that is 0.0026% of the pulse width. The average D_t value found for the reflection case in figure 6(b) is -0.14 ±0.12 ns or a 0.0091% temporal shift. We see that it is indeed possible to achieve $D_t = 0$ for chirped pulses over a broad range of center frequencies. We found for pulses with a frequency bandwidth around 5 MHz, that the uncertainty in the time shift is around ±0.12 ns and the uncertainty in the calculated frequency shift is approximately ±0.6 kHz. The error bars on the shift in time is shown in figure 6, whereas we do not place error bars on the frequency shift measurements because the uncertainty is smaller than the size of the data symbol.

Achieving $D_t \approx 0$ was significantly more difficult for the reflection case, where we were only able to achieve well behaved $D_t \approx 0$ behavior near resonance. When looking off resonance at the imaginary part of reflection time delay (shown in figure 6(b)) we see that there are multiple zero crossings and that in general the imaginary part tends to hover around zero. Since we are imposing $\Omega'\delta_t^2 = \mathrm{Re}[\tau]/\mathrm{Im}[\tau]$ we expect there to be divergences in chirp parameter when $\mathrm{Im}[\tau] = 0$. The full data set is located in figure 4 of the Supp Mat, where we see sharp increases in D_t where $\mathrm{Im}[\tau] = 0$. Additionally, see figure 3 in the Supp Mat where we perform this same study with pulses having considerably wider (50–70 MHz) frequency bandwidth.

5. Conclusion

In this paper we have established a comprehensive theoretical and experimental framework connecting CTD to the properties of linearly chirped pulses traveling through linear and dispersive non-Hermitian resonant scattering systems. Building upon the work in [44, 69], we have demonstrated that both the real and imaginary components of CTD play essential roles in determining chirped pulse behavior, with the imaginary part contributing not only to the observed frequency shifts but also to the temporal shifts weighted by the chirp parameter $\Omega'\delta_t^2$. As a result, this work broadens not only how we physically interpret CTD [35, 39] but also adds further motivation for why it is useful to generalize real time delay to non-Hermitian systems in the first place.

The experimental validation for both cases of transmission and reflection, spanning a wide range of chirp rates (both positive and negative) and pulse frequency bandwidths, confirms the robustness of our theoretical predictions and their practical utility. This allows one to construct chirped pulses with predetermined temporal and spectral characteristics using only knowledge of the system's transmission or reflection coefficient as a function of frequency. This was demonstrated in figure 6 where we used the resonator's transmission/reflection coefficient to appropriately choose the chirp rate and pulse duration such that the time shift D_t of the pulse is nullified over a wide frequency range. The ability to achieve near-zero broadband time shifts opens new possibilities for precision control in various applications ranging from pulse compression systems to quantum computing. This result also represents a new way to take advantage of the additional degrees of freedom present in chirped pulses, going beyond what is achievable with unchirped pulses alone.

Looking ahead, there are several interesting avenues for future work. Extension to multi-mode systems with overlapping resonances would test how our theory holds in more realistic environments where mode coupling and interference effects become important. Similarly, it would be interesting to see how our theory can be expanded to systems with more than two ports or for nonlinearly chirped pulses. Additionally, since in this paper we only used simple microwave ring resonators, it would be valuable to examine how a resonator's geometry or characteristics (i.e. coupling strength, loss, Q-factor, etc) impact the achievable range for D_t and D_f. Another open question would be how these results translate to the optical domain using systems such as an optical ring resonator or a whispering gallery mode resonator.

Data availability statement

The data that support the findings of this study are openly available at the following URL/DOI: http://hdl.handle.net/1903/35326 [70].

Supplementary Material available at https://doi.org/10.1088/2515-7647/ae7b9b/data1.

Funding

This work was partially supported by NSF/RINGS under grant No. ECCS-2148 318, ONR under Grant N000142312507, and DARPA WARDEN under Grant HR00112120021.

Disclosures

The authors declare no conflicts of interest.

ORCID iDs

Isabella L Giovannelli 0009-0009-1772-2177
Steven M Anlage 0000-0001-7850-9059
Thomas M Antonsen 0000-0002-2362-2430

References

[1] Strickland D and Mourou G 1985 Compression of amplified chirped optical pulses *Opt. Commun.* **56** 219–21
[2] Kaltenbaek R, Lavoie J, Biggerstaff D N and Resch K J 2008 Quantum-inspired interferometry with chirped laser pulses *Nat. Phys.* **4** 864–8
[3] Bérubé M M, Mazurek M D and Resch K J 2025 Enhanced-resolution chirped-pulse interferometry *Phys. Rev. A* **112** 023525
[4] Park G B and Field R W 2016 Perspective: The first ten years of broadband chirped pulse fourier transform microwave spectroscopy *J. Chem. Phys.* **144** 200901
[5] Markmann S, Franckié M and Bertrand M *et al* 2023 Frequency chirped fourier-transform spectroscopy *Commun. Phys.* **6** 53
[6] Allen C, Cobanoglu Y, Chong S K and Gogineni S 2001 Performance of a 1319 nm laser radar using RF pulse compression *IGARSS 2001. Scanning the Present and Resolving the Future. Proc. IEEE 2001 Int. Geoscience and Remote Sensing Symp. (Cat. No.01CH37217)* vol 3 pp 997–9
[7] Adany P, Allen C and Hui R 2009 Chirped Lidar using simplified homodyne detection *J. Lightwave Technol.* **27** 3351–7
[8] Saperstein R E, Alic N, Zamek S, Ikeda K, Slutsky B and Fainman Y *et al* 2007 Processing advantages of linear chirped fiber Bragg gratings in the time domain realization of optical frequency-domain reflectometry *Opt. Express* **15** 15464
[9] Piracha M U, Nguyen D, Ozdur I and Delfyett P J 2011 Simultaneous ranging and velocimetry of fast moving targets using oppositely chirped pulses from a mode-locked laser *Opt. Express* **19** 11213
[10] Darlington S 1954 U.S.Patent No.2,678,997
[11] Klauder J R, Price A C, Darlington S and Albersheim W J 1960 Theory and design of chirp radars *Bell Syst. Tech. J.* **39** 745–808
[12] Lihachev G *et al* 2022 Low-noise frequency-agile photonic integrated lasers for coherent ranging *Nat. Commun.* **13** 3522
[13] Lukashchuk A *et al* 2024 Photonic-electronic integrated circuit-based coherent LiDAR engine *Nat. Commun.* **15** 3134
[14] Chong A, Buckley J, Renninger W and Wise F 2006 All-normal-dispersion femtosecond fiber laser *Opt. Express* **14** 10095–100
[15] Wise F, Chong A and Renninger W 2008 High-energy femtosecond fiber lasers based on pulse propagation at normal dispersion *Laser Photonics Rev.* **2** 58–73
[16] Cao Q, Chen J and Lu K *et al* 2021 Sculpturing spatiotemporal wavepackets with chirped pulses *Photon. Res.* **9** 2261–4
[17] Katz O, Small E, Bromberg Y and Silberberg Y 2011 Focusing and compression of ultrashort pulses through scattering media *Nat. Photon.* **5** 372–7
[18] Snigirev V *et al* 2023 Ultrafast tunable lasers using lithium niobate integrated photonics *Nature* **615** 411–7
[19] Kumar C, Raghuwanshi S K and Yadav R K 2024 A review on photonic-assisted dual-chirp microwave waveform generation methods *Microw. Opt. Technol. Lett.* **66** e34266
[20] Delfyett P J, Mandridis D, Piracha M U, Nguyen D, Kim K and Lee S *et al* 2012 Chirped pulse laser sources and applications, *Prog. Quantum Electron.* **36** 475–540
[21] Hofmann C, Landsman A S and Keller U 2019 Attoclock revisited on electron tunnelling time *J. Mod. Opt.* **66** 1052–70
[22] Yusoff M A H B M and Djiokap J M N 2024 Time-delay control of reversible electron spirals using arbitrarily chirped attosecond pulses *Phys. Rev. A* **109** 023107
[23] Vincenti H and Quéré F 2012 Attosecond lighthouses: how to use spatiotemporally coupled light fields to generate isolated attosecond pulses *Phys. Rev. Lett.* **108** 113904
[24] Hawkins P E, Malinovskaya S A and Malinovsky V S 2012 Ultrafast geometric control of a single qubit using chirped pulses *Phys. Scr.* **T147** 014013
[25] Kuzmanović M, Björkman I, McCord J J, Dogra S and Paraoanu G S 2024 High-fidelity robust qubit control by phase-modulated pulses *Phys. Rev. Res.* **6** 013188
[26] O'Sullivan J, Kennedy O W and Debnath K *et al* 2022 Random-Access Quantum Memory Using Chirped Pulse Phase Encoding *Phys. Rev. X* **12** 041014

[27] Ouyang X and Zhao J 2016 Orthogonal chirp division multiplexing *IEEE Trans. Commun.* **64** 3946–57
[28] Li X, Zhao S, Wang G and Zhou Y 2021 Photonic generation and application of a bandwidth multiplied linearly chirped signal with phase modulation capability *IEEE Access* **9** 82618–29
[29] Malinovskaya S A and Malinovsky V S 2007 Chirped-pulse adiabatic control in coherent anti-Stokes Raman scattering for imaging of biological structure and dynamics *Opt. Lett.* **32** 707
[30] Malinovskaya S 2007 Chirped pulse control methods for imaging of biological structure and dynamics *Int. J. Quantum Chem.* **107** 3151–8
[31] Mamou J, Ketterling J A and Silverman R H 2008 Chirp-coded excitation imaging with a high-frequency ultrasound annular array *IEEE Trans, Ultrason. Ferroelectr. Freq. Control* **55** 508–13
[32] Niederriter R D, Ozbay B N and Futia G L *et al* 2017 Compact diode laser source for multiphoton biological imaging *Biomed. Opt. Express* **8** 315–22
[33] de Boer J F, Leitgeb R and Wojtkowski M 2017 Twenty-five years of optical coherence tomography: the paradigm shift in sensitivity and speed provided by fourier domain oct [invited] *Biomed. Opt. Express* **8** 3248–80
[34] Popoff S M, Lerosey G, Carminati R, Fink M, Boccara A C and Gigan S 2010 Measuring the transmission matrix in optics: An approach to the study and control of light propagation in disordered media *Phys. Rev. Lett.* **104** 100601
[35] Chen L and Anlage S M 2022 Use of transmission and reflection complex time delays to reveal scattering matrix poles and zeros: Example of the ring graph *Phys. Rev. E* **105** 054210
[36] Eisenbud L 1948 The formal properties of nuclear collisions *PhD Thesis* Princeton University
[37] Wigner E P 1955 Lower limit for the energy derivative of the scattering phase shift *Phys. Rev.* **98** 145–7
[38] Smith F T 1960 Lifetime matrix in collision theory *Phys. Rev.* **118** 349–56
[39] Chen L, Anlage S M and Fyodorov Y V 2021 Generalization of Wigner time delay to subunitary scattering systems *Phys. Rev. E* **103** L050203
[40] El-Ganainy R, Makris K G, Khajavikhan M, Musslimani Z H, Rotter S and Christodoulides D N 2018 Non-Hermitian physics and PT symmetry *Nat. Phys.* **14** 11–19
[41] Ozdemir S K, Rotter S, Nori F and Yang L 2019 Parity-time symmetry and exceptional points in photonics *Nat. Mater.* **18** 783–98
[42] Ashida Y, Gong Z and Ueda M 2020 Non-Hermitian physics *Adv. Phys.* **69** 249–435
[43] Xue P 2026 Essay: topological phases and exceptional points in non-Hermitian systems *Phys. Rev. Lett.* **136** 170001
[44] Asano M *et al* 2016 Anomalous time delays and quantum weak measurements in optical micro-resonators *Nat. Commun.* **7** 13488
[45] del Hougne P, Yeo K B, Besnier P and Davy M 2021 On-demand coherent perfect absorption in complex scattering systems: Time delay divergence and enhanced sensitivity to perturbations *Laser Photonics Rev.* **15** 2000471
[46] Huang Y, Kang Y and Genack A Z 2022 Wave excitation and dynamics in non-Hermitian disordered systems *Phys. Rev. Res.* **4** 013102
[47] Shaibe N, Erb J M and Anlage S M 2025 Superuniversal statistics of complex time delays in non-Hermitian scattering systems *Phys. Rev. Lett.* **134** 147203
[48] Bender C M and Boettcher S 1998 Real spectra in non-Hermitian hamiltonians having PT symmetry *Phys. Rev. Lett.* **80** 5243–6
[49] Ruschhaupt A, Simon M A, Kiely A and Muga J G 2021 The role of symmetry in non-Hermitian scattering *J. Phys.: Conf. Ser.* **2038** 012020
[50] Shaibe N, Erb J M and Anlage S M 2025 Superuniversal statistics with topological origins for non-Hermitian scattering singularities *Phys. Rev. Res.* **7** 043185
[51] Ambichl P, Brandstötter A, Böhm J, Kühmayer M, Kuhl U, Rotter S 2017 Focusing inside disordered media with the generalized Wigner-Smith operator *Phys. Rev. Lett.* **119** 033903
[52] Bliokh K Y, Kuang Z and Rotter S 2025 Dynamic and geometric shifts in wave scattering *Rep. Prog. Phys.* **88** 107901
[53] Byrnes N and Foreman M R 2025 Generalized Wigner-Smith analysis of resonance perturbations in arbitrary Q non-Hermitian systems *Phys. Rev. Res.* **7** 013299
[54] Byrnes N and Foreman M R 2025 Perturbing scattering resonances in non-Hermitian systems: A generalized Wigner-Smith operator formulation *Newton* **1** 100194
[55] Garrett C G B and McCumber D E 1970 Propagation of a Gaussian Light pulse through an anomalous dispersion medium *Phys. Rev. A* **1** 305–13
[56] Crisp M D 1971 Concept of group velocity in resonant pulse propagation *Phys. Rev. A* **4** 2104–8
[57] Chu S and Wong S 1982 Linear Pulse Propagation in an Absorbing Medium *Phys. Rev. Lett.* **48** 738–41
[58] Boyd R W and Gauthier D J 2002 Slow and fast light *Progress in Optics* ed E Wolf (Elsevier Science)
[59] Gehring G M, Schweinsberg A, Barsi C, Kostinski N and Boyd R W 2006 Observation of Backward Pulse Propagation Through a Medium with a Negative Group Velocity *Science* **312** 895–7
[60] Bortolozzo U, Residori S and Huignard J P P 2010 Slow and fast light: basic concepts and recent advancements based on nonlinear wave-mixing processes *Laser Photonics Rev.* **4** 483–98
[61] Stenner M D, Gauthier D J and Neifeld M A 2003 The speed of information in a 'fast-light' optical medium *Nature* **425** 695–8
[62] Sommerfeld V A 1907 Concerning the alternating current resistance of coils *Phys. Z.* **8** 805–9
[63] Brillouin L 1914 Über die fortpflanzung des lichtes in dispergierenden medien (On the propagation of light in dispersive media) *Ann. Physik* **44** 203–40
[64] Brillouin L and Sommerfeld A 1960 *Wave Propagation and Group Velocity* (Academic) ch 2, pp 17–39
[65] Thompson K, Li K, Angulo D, Nixon V-M, Sinclair J, Sivakumar A V, Wiseman H M and Steinberg A M 2025 How much time does a photon spend as an atomic excitation before being transmitted through a cloud of atoms? *APL Quantum* **2** 036108
[66] Angulo D, Thompson K, Nixon V M, Jiao A, Wiseman H M and Steinberg A M *et al* 2026 Experimental observation of negative weak values for the time atoms spend in the excited state as a photon is transmitted *Phys. Rev. Lett.* **136** 153601
[67] Cao H, Dogariu A and Wang L 2003 Negative group delay and pulse compression in superluminal pulse propagation *IEEE J. Sel. Top. Quantum Electron.* **9** 52–58
[68] Waltner D and Smilansky U 2013 Scattering from a ring graph - a simple model for the study of resonances *Acta Phys. Pol. A* **124** 1087–90
[69] Giovannelli I L and Anlage S M 2025 Physical interpretation of imaginary time delay *Phys. Rev. Lett.* **135** 043801
[70] Giovannelli I 2026 Dataset for "Chirped Pulse Analysis and Control in Non-Hermitian Scattering Systems using Complex Time Delay" manuscript *Digital repository at the University of Maryland* (available at: http://hdl.handle.net/1903/35326)